EXPERIMENTAL CHARACTERIZATION OF THERMAL PERFORMANCE OF FLAT PLATE SOLAR COLLECTORS WITH ROLL-BOND ABSORBERS

Davide Del Col, Marco Dai Prè, Matteo Bortolato and Andrea Padovan

Università degli Studi di Padova, Dipartimento di Fisica Tecnica

Via Venezia 1, 35131 Padova, Italy, tel: +39 0498276896, email: davide.delcol@unipd.it

Abstract

In this work, a new prototype of glazed flat plate solar collector is presented and its performance is experimentally characterized. The new collector uses a roll-bond absorber plate made of aluminum. The roll-bond is a production process aimed at manufacturing canalized panels by bonding two aluminum sheets with a rolling technique. Thus, in this prototype, the channels for liquid are integrated in the absorber plate.

Measurements of thermal efficiency are reported for two prototypes, one with a black coating and the other with a semi-selective coating and those measurements are compared with those of standard glazed flat plate collectors at the same test conditions. The test runs have been performed in several conditions in order to reproduce different uses: hot water, space heating and solar cooling. The effect of the coating of the absorber is also evaluated and discussed using the experimental data collected. Efficiency test runs have been performed on a test rig both in steady-state and in quasi-dynamic conditions, according to the standard EN 12975-2 (2006). The results are presented in terms of efficiency curves.

A three-dimensional model is used to predict the behavior in steady-state conditions of the solar collectors to obtain the efficiency curve. The model was implemented for standard glazed flat plate collectors but, in this work, its use is extended to roll-bond solar collectors and its validation is made by the comparison with the efficiency curve obtained from experimental tests.

1. Introduction

Glazed flat-plate solar collectors are the most widely used devices to convert solar radiation in many Countries. They usually present a metal absorber sheet (few tenths of millimeter thick) where metal tubes are welded, an upper glass cover and an insulation layer on the back side. Air is present in the space between the plate absorber and the glass cover. All these elements are accommodated in a flat rectangular housing. This simple geometry allows the absorption of the incident solar radiation and the transfer of the retained heat flux to the working fluid flowing inside the tubes, minimizing the amount of heat flux wasted to the surrounding environment.

In this work, a new prototype of glazed solar collector with a roll-bond absorber plate made of aluminum is presented. Roll-bond technology is widely employed for the manufacturing of heat exchangers, such as evaporators for the domestic refrigeration, radiant panels, cryostatic circuits, cooling system for photovoltaic modules. In general, roll-bond is a process aimed at manufacturing canalized panels applying a special bonding technique: a sandwich of two aluminum sheets is formed by a special hot/cold rolling process. Before bonding together the aluminum sheets, on the inner surface of one sheet, the desired pattern of channels is printed with a serigraphic process, using a special ink, which prevents the welding of the inner surfaces where it is applied. Finally, the unbounded pattern of channels has to be lifted up inflating air at very high pressure and the panels are completed with connections. As a consequence, a roll-bond solar collector presents channels for working fluids integrated in the absorber plate (1-2 mm thick). It is reasonable to think that this main feature allows to a more uniform temperature distribution on the absorber with respect to the standard flat plate collectors.

In this paper the authors present a new set of data collected at Padua, Italy (45° 25’ N, 11° 53’E): both standard flat plate collectors with black and selective coating and roll-bond collectors with black and semi-

selective coating are tested at the same conditions following the steady-state efficiency test and the quasi-dynamic efficiency test described by the standard EN 12975-2.

Moreover, in this work, the three dimensional model described in Zambolin and Del Col (2010a) has been applied to the standard solar collectors and has been adapted for the roll-bond solar collectors. The model has been validated against experimental data collected. In the model, the edge losses are considered, the thermo-physical properties of collector insulation and working fluid are dependent on the temperature and the effect of axial and transversal (referred to mass flow direction) conduction are accounted for.

2. Experimental apparatus

The experimental apparatus is located on the terrace roof of the Dipartimento di Fisica Tecnica of the University of Padua and has been set up to allow the measurement of solar collectors efficiency in agreement with the main guidelines of the standard EN 12975-2 (Zambolin and Del Col, 2010b). It includes a hydraulic loop and the instrumentation for the measurement of mass flow rate, inlet and outlet fluid temperature, solar irradiance, wind speed and ambient air temperature.

The hydraulic loop is divided into two lines that allow the measurement of efficiency of two solar collectors in parallel. A scheme of the hydraulic loop is reported in Fig.1.. Each line includes a pump to circulate water, which is the working fluid. A Coriolis effect and a magnetic type flow meters are used to measure the water flow rate. The second instrument measures a volumetric flow rate, but the density of the fluid can be easily calculated. The liquid temperature at the inlet of the collectors is controlled by a temperature sensor inserted in storage 2, where four electrical heaters are located. Three heaters have an electrical power of 5 kW and the heater at the bottom of the storage has an adjustable power from 0 to 5 kW. According to the desired total flow rate, it is possible to set the electrical power to obtain a certain inlet temperature of the liquid. The liquid temperature both at the inlet and at the outlet of each solar collector is measured by platinum resistance thermometers (RTDs). The fluid coming from the collectors enters the storage 1 and then goes to a plate heat exchanger that works as a heat sink. In the heat exchanger, the heat flow rate provided by the solar radiation is taken away by a secondary fluid and then wasted in a second exchanger to the ground water of the building central plant.

Three solar collectors have been installed in subsequent test campaigns: a glazed flat plate collector provided with copper absorber with a black coating and copper tubes (Fig. 2, left), a glazed flat plate roll-bond collector with black coating and a glazed flat plate roll-bond collector with semi-selective coating (Fig. 2, right). The collectors are oriented 10° south-west and during the tests they are tilted of 60° in order to meet the incidence angle requirement of the standard EN 12975-2.

In table 1, some characteristics of the collectors installed here are reported.

The instrumentation includes three all black thermopile based pyranometers to measure the solar irradiance. A Kipp&Zonen pyranometer, classified as secondary standard by the World Meteorological Organization (WMO) is mounted at the midheight and on the same plane of the collectors to measure the global solar irradiance on the tilted plane. Another Kipp&Zonen pyranometer, classified as secondary standard, measures the global solar irradiance on the horizontal plane and a third Delta Ohm pyranometer (first class classified) is provided with a shading band to measure the diffuse component on the horizontal plane.

The Drummond model (Drummond, 1956) is used for the correction required for the shading band to determine the effective diffuse irradiance on the horizontal plane. The Liu and Jordan method (Liu and Jordan, 1963) is then used to calculate the direct irradiance on the tilted plane of the collectors, from the direct irradiance on the horizontal plane that is obtained from the difference between the global and the diffuse irradiance on the horizontal plane. A platinum resistance thermometer is used to measure the ambient air temperature and an anemometer measures the air speed, which influences the heat loss from collector.

In table 2, the uncertainty of the transducers installed in the experimental apparatus is reported. The percentages in this table are referred to the measured values.

Table 1: Characteristics of the collectors installed in the test rig

	Unit	Standard flat plate collector Copper absorber with black coating Copper tubes	Roll-bond flat plate collector Black coating	Roll-bond flat plate collector Semi-selective coating
Gross area	m^2	2.016	2.016	2.016
Aperture area	m^2	1.810	1.810	1.810
Number of flow channels in parallel		10	28	28
Absorber thickness	mm	0.12	1.5	1.5
Absorber emittance		0.96	0.96	0.35
Absorber absorbance		0.96	0.96	0.87

Table 2: Uncertainty of transducers at typical test conditions

Fluid temperature	±0.05 K
Ambient air temperature	±0.1 K
Coriolis effect mass flow meter	±0.1%
Magnetic type flow meter	±0.25%
Solar irradiance	Secondary standard sensor (collector plane and global irradiance on horizontal plane) First class sensor (diffuse irradiance on horizontal plane)
Air speed	± 0.1m/s+1%

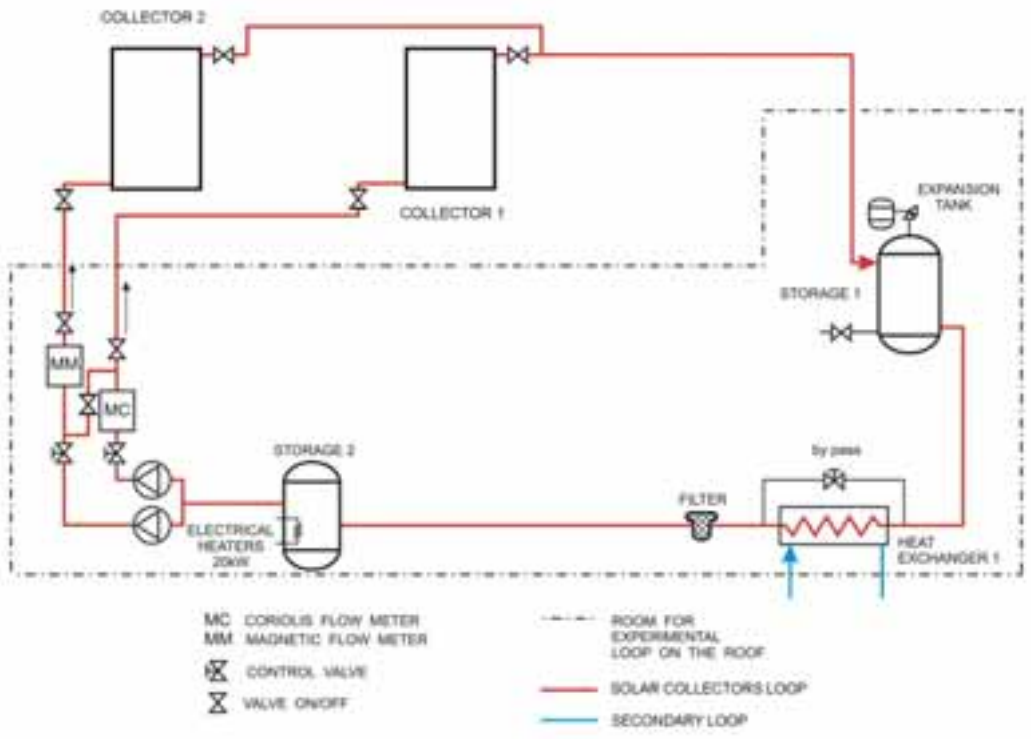

Fig. 1: Schematic view of the experimental test rig

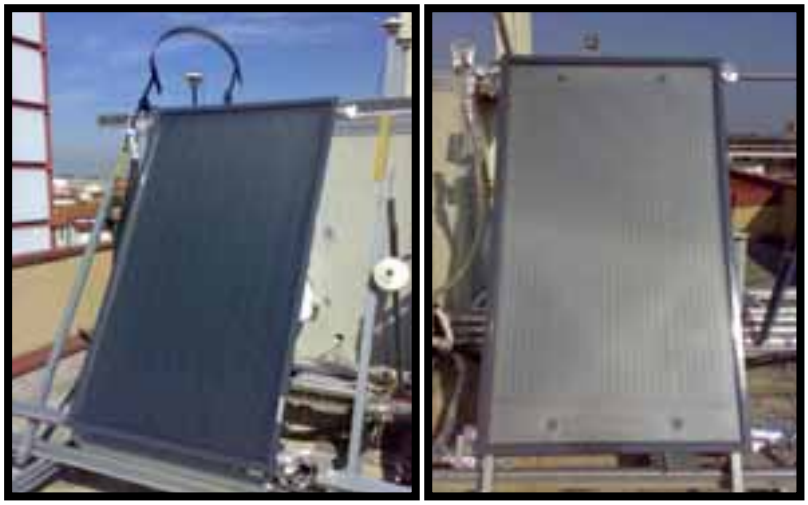

Fig 2. Some of the solar collectors tested; left: glazed flat plate solar collector with copper absorbed with black coating and copper tubes; right: glazed flat plate collector with a roll-bond plate as absorber and selective coating.

3. Experimental results and discussion

3.1 Efficiency in steady-state conditions

According to the EN 12975-2, a collector is considered to operate in steady-state conditions over a given measurement period if the experimental parameters deviate from their mean values within the limits reported in Table 3. When operating in steady-state conditions, the useful output power of a solar collector for near normal incidence angle of the solar irradiance can be described by the following equation (Duffie and Beckman, 2006):

$$\dot{Q} = F' \cdot A_a \cdot (\tau\alpha)_{en} \cdot G - U \cdot (t_m - t_a) \qquad \text{(eq. 1)}$$

where $\dot{Q}$ is the useful output power transferred to the liquid, *F'* the collector efficiency factor, A_a the aperture area, $(\tau\alpha)_{en}$ the effective transmittance-absorbance product at normal incidence, *G* the global solar irradiance, *U* the overall heat loss coefficient and (t_m-t_a) the difference between the average fluid temperature in the collector and the ambient air temperature.

In consequence, the efficiency is equal to

$$\eta = \frac{\dot{Q}}{G \cdot A_a} = F' \cdot \left[(\tau\alpha)_{en} - U \cdot \frac{(t_m - t_a)}{G} \right] = F' \cdot (\tau\alpha)_{en} - U \cdot T_m^* \qquad \text{(eq. 2)}$$

where T_m^* is the reduced temperature difference.

The equation provided in the standard EN 12975-2 for efficiency steady-state tests is derived from eq. 2, considering the heat loss coefficient as the sum of a constant factor and a term dependent on the temperature difference between fluid and ambient air and it is presented as follows:

$$\eta = \eta_0 - a_1 \cdot T_m^* - a_2 \cdot G \cdot T_m^{*\,2} \qquad \text{(eq.3)} .$$

The regression curve parameters have been obtained by multiple linear regression, following the procedure reported in the standard EN12975-2, by developing a process in Matlab environment.

Table 3: Test conditions and permitted deviation of measured parameters during a measurement period for steady-state tests according to EN12975.

Experimental parameter	Value	Deviation from the mean value
Global irradiance G (W m^{-2})	>700	
Diffuse fraction G_d /G	<30	
Incidence angle beam irradiance (°)	<20°	
Inlet fluid temperature		± 0.1
Surrounding air speed (m/s)	from 1 to 3	
Surrounding air temperature (°C)		±1.5
Fluid mass flow rate	0.02 kg/s per square meter of collector aperture area	±1%

3.2 Efficiency in quasi-dynamic conditions

The standard EN 12975 provides an alternative test method for the characterization of a solar collector: the quasi-dynamic method. It allows to achieve comparable results of the steady-state method even at less stable meteorological and operating conditions (Table 4). Consequently, a complete characterization of a solar with the quasi-dynamic method collector can be obtained in fewer days.

The collector model is basically the same as steady-state model, but with some correction terms: in the EN 12975-2, the energy balance for the quasi-dynamic method (eq. 4) includes the dependence of direct and diffuse irradiance, wind speed, sky temperature, long wave irradiance, incidence angle effects and effective thermal capacitance.

$$\frac{\dot{Q}}{A_a} = F' (\tau\alpha)_{en} \cdot K_{\theta b} \cdot G_b + F' \cdot (\tau\alpha)_{en} \cdot K_{\theta d} \cdot G_d - c_6 \cdot u \cdot G - c_1 \cdot (t_m - t_a) - c_2 \cdot (t_m - t_a)^2 - c_3 \cdot u \cdot (t_m - t_a) + c_4 \cdot (E_L - \sigma T_a^4) - c_5 \cdot \frac{dt_m}{d\tau} \quad \text{(eq.4)}$$

$K_{\theta b}$ and $K_{\theta d}$ are the collector incidence angle modifiers for direct radiation and diffuse radiation, respectively. For flat plate collectors, $K_{\theta b}$ is defined by (eq.5), where b_0 is the incidence angle modifier coefficient and has a negative value while $K_{\theta d}$ should be modeled as a constant.

$$K_{\theta b} = 1 - b_0 \cdot \left(\left(\frac{1}{\cos\theta} \right) - 1 \right) \quad \text{(eq.5)}$$

The efficiency derives from (eq.4), using the value of G = 1000 W/m^2 and a diffuse fraction of 15%, that is to say G_d = 150 W/m^2. Moreover, the parameter $dt_m/d\tau$ is set to zero and $K_{\theta b}$ is calculated for θ = 15° and the wind and the long wave irradiance effects can be neglected for glazed solar collectors. The final expression is reported in (eq.6). The model parameters and their uncertainty are calculated with the weighted least square (WLS) method, as shown in EN 12975-2.

$$\eta = F' (\tau\alpha)_{en} \cdot K_{\theta b}(15°) \cdot 0.85 + F' (\tau\alpha)_{en} \cdot K_{\theta d} \cdot 0.15 - C_1 \cdot T_m^* - C_2 \cdot G \cdot T_m^{*2} \quad \text{(eq.6)}$$

3.3 Experimental results

The tests have been performed in agreement with the guidelines of the standard EN 12975, apart from the measurement of the wind speed, which was measured on the horizontal plane and not on the collector's plane. The procedure has been repeated varying the inlet fluid temperature and finally the results are reported in diagrams plotting the efficiency against the reduced temperature difference. The efficiency curves plotted

in the diagrams are all referred to a global irradiance G = 1000 W/m^2. In the efficiency curves obtained in steady-state conditions the experimental points are also present. For each point, the experimental uncertainties of the measured efficiency and the reduced temperature difference (95% confidence interval) are reported, as calculated following the instructions provided in ISO (1995) and described in Kratzenberg et al. (2006) for the measured efficiency. The results for each collector are presented in Fig. 3 – 5. From the comparisons between the curves obtained in steady-state and in quasi-dynamic conditions and reported for the same irradiance conditions, it can be observed that the results obtained by these different procedures are fully compatible within their error ranges.

The parameters of the efficiency curves and their regression uncertainties, determined from the steady-state and quasi-dynamic procedures, for the four collectors are listed in Table 5 and in Table 6. The plotted efficiency curves are referred to the aperture area of the collectors. In this tables the uncertainties of the target parameters are obtained as the square root of the variances, determined as reported in the procedure described in Kratzenberg et al. (2006) in the case of the weighted least square (WLS) method (only the variances are considered because all the collector coefficients are uncorrelated).

Table 4: Test conditions and permitted deviation of measured parameters for the quasi-dynamic method according to EN12975.

Experimental parameter	Value	Deviation from the mean value
Global irradiance G (W/m^2)	Lower limit not specified	
	(>150 in present test)	
Inlet fluid temperature		$\pm$ 1
Surrounding air speed (m/s)	from 1 to 4	
Fluid temperature difference (°C)	>1	
Fluid mass flow rate	0.02 kg/s	$\pm$1%
	per square meter of collector aperture area	

Table 5: Collector coefficients obtained with quasi-dynamic and steady-state methods for the roll-bond flat plate collectors.

	Black coating				Semi-selective coating			
	Quasi-dynamic test		Steady-state test		Quasi-dynamic test		Steady-state test	
Parameter	Value	Uncertainty	Value	Uncertainty	Value	Uncertainty	Value	Uncertainty
$F'(\tau\alpha)_{en}\ \eta_0$ *(sst)*	0.8419	±0.0168	0.7995	±0.0108	0.7558	±0.0188	0.7409	±0.0110
b_0	0.6803	±0.6342			0.1788	±0.1515		
$K_{\theta d}$	0.8340	±0.0905			0.8749	±0.0985		
c_1 *[W/(m^{2}K)]*	5.9607	±0.9398	4.6911	±0.7879	4.2533	±1.1823	4.5477	±0.6865
c_2 *[W/(m^{2}K)]*	0.0131	±0.0155	0.0288	±0.0121	0.0175	±0.0178	0.0131	±0.0100
c_5 *[J/(m^{2}K)]*	10642	±5106.5			14818	±5349.6		

Table 6: Collector coefficients obtained with quasi-dynamic and steady-state methods for the standard flat plate collector.

	Black coating			
	Quasi-dynamic test		Steady-state test	
Parameter	Value	Uncertainty	Value	Uncertainty
$F'(\tau\alpha)_{en}\ \eta_0$ (sst)	0.7135	±0.0157	0.6925	±0.0084
b_0	0.1510	±0.2156		
$K_{\theta d}$	0.8695	±0.0869		
c_1 *[W/(m^{2}K)]*	5.2719	±0.9955	4.6804	±0.5577
c_2 *[W/(m^{2}K)]*	0.0087	±0.0154	0.0174	±0.0083
c_5 *[J/(m^{2}K)]*	12328	±5261.5		

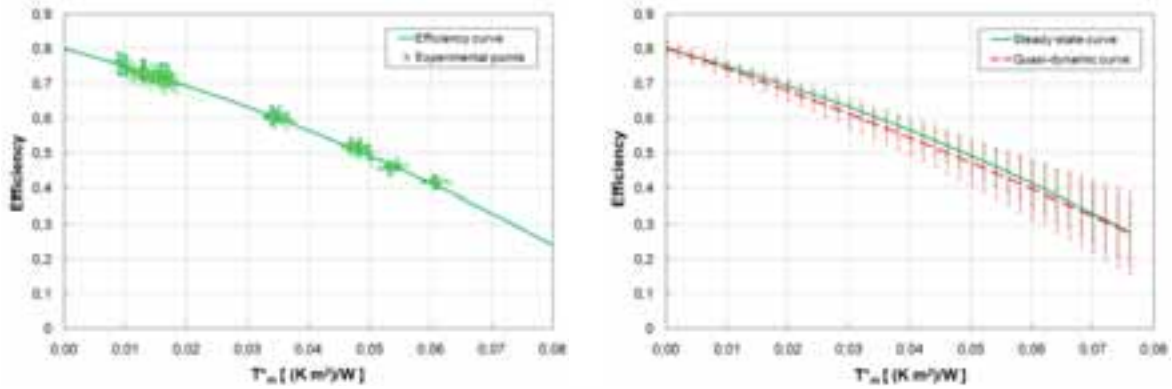

Fig. 3: Roll-bond collector with black coating. Left: efficiency curve at G = 1000 W/m^2 and experimental points obtained in steady-state condition. Right: compared efficiency curves in steady-state and quasi-dynamic condition at G = 1000 W/m^2.

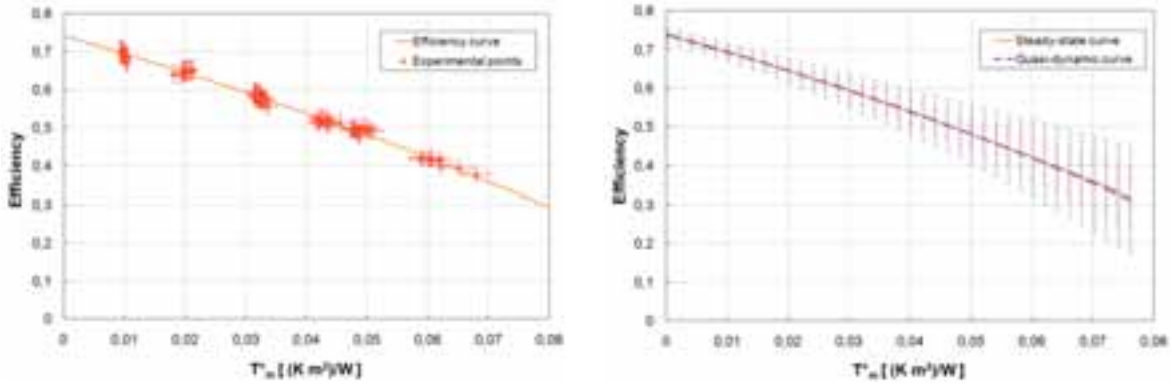

Fig. 4: Roll-bond collector with semi-selective coating. Left: efficiency curve at G = 1000 W/m^2 and experimental points obtained in steady-state condition. Right: compared efficiency curves in steady-state and quasi-dynamic condition at G = 1000 W/m^2.

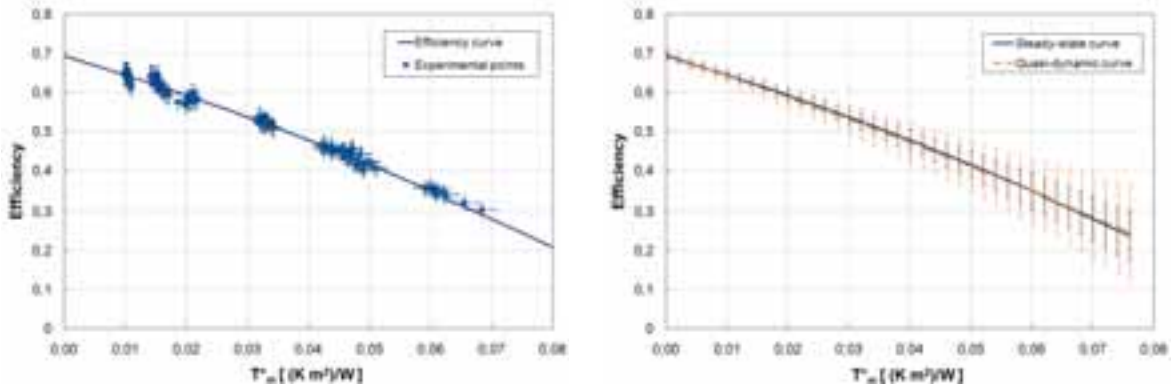

Fig. 5: Standard collector with black coating. Left: efficiency curve at G = 1000 W/m^2 and experimental points obtained in steady-state condition. Right: compared efficiency curves in steady-state and quasi-dynamic condition at G = 1000 W/m^2.

In Fig. 6, the comparison between the performances of the tested collectors is presented. The comparison has been done with the curves obtained in steady-state condition referred to a global irradiance G = 1000 W/m^2.

The comparison between the two collectors with black coating shows that the performance of the roll-bond collector is better than the performance of the standard flat plate collector with copper absorber plate and copper tubes. The efficiency curves cross when T^*_m = 0.096 (K m^2)/W, which is a very high value for the common application for the flat plate collectors, such as production of hot water for heating or for domestic use. The comparison between the two roll-bond collectors shows that the performance of the collector with

black coating is higher than the performance of the collector with semi-selective coating until T^*_m = 0.058 K m^2/W.

The semi-selective coating present a low absorbance (0.87, while the black coating present 0.96) and the lower emittance (0.35 instead 0.96 of the black coating) recovers the initial gap of the efficiency only when the reduced temperature difference is high (for the traditional uses of the flat plate collectors).

In Fig.7, a comparison between the performance of the roll-bond collector with black painting and a reference standard collector Riello CP20TS with selective coating (Test report SPF,2008) is depicted. The coefficients of the efficiency curve of the reference collector are reported in Table 7.

It can be noticed that the performance of the roll-bond collector is above the reference collector until T^*_m = 0.035 K m^2/W.

Table 7: Coefficients and aperture area of reference standard collector Riello CP20TS with selective coating (Test report SPF, 2008)

Reference standard collector with selective coating	
Parameter	Value
η_0 (sst)	0.748
a_1 [W/(m^{2}K)]	3.82
a_2 [W/(m^{2}K)]	0.0101
A_a [m^2]	1.804

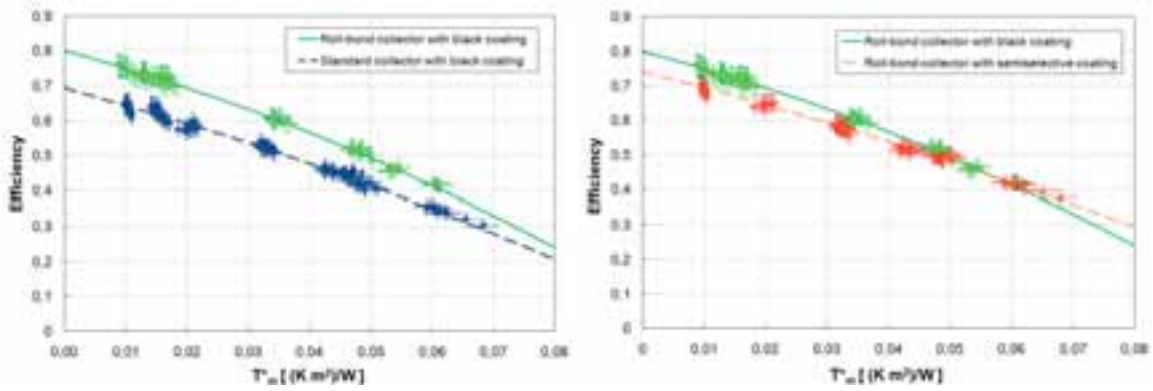

Fig. 6: Compared efficiency curves in steady-state condition at G = 1000 W/m^2. Left: the roll-bond and the standard collector with black coating; right: the two roll-bond collectors.

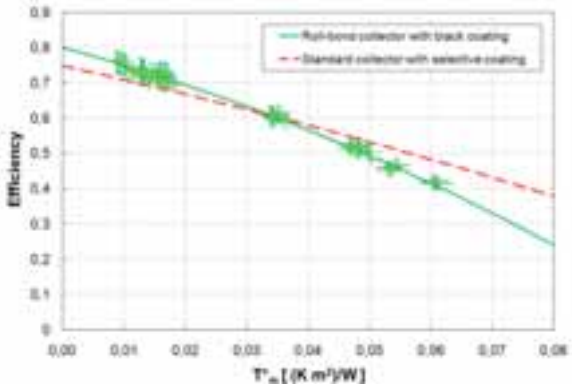

Fig. 7: Compared efficiency curves in steady-state condition at G = 1000 W/m^2: roll-bond collector with black coating vs reference standard collector with selective coating.

4. Computational model

The solar collector is modeled as a series of overlapping parts: the back insulation, the absorber plate, the air gap and the glass cover. The absorber is the core component of the system and it is exposed to an input heat flux due to the incident solar irradiance. The heat loss transfer is obtained from the energy balance between each other component, where the driving force is the temperature difference between the plate and the external surroundings.

The absorber plate has been divided in two-dimensional control elements so that the elements that are not at the edge of the plate present an elementary part of tube in the center. The computational analysis is based on the hypothesis of steady-state conditions and it is divided in two different steps: at first, the simulation does not take into account the thermal conduction between different control elements; in the second step, the conduction is calculated using a temperature map previously obtained. The useful heat flux in a control element (length *dx* and width *w*) can be written as:

$$q_{u\_x,y} = \Theta \cdot \dot{m} \cdot c_p \cdot \left(t_{out\_x,y} - t_{in\_x,y} \right) \qquad \text{(eq.7)}$$

where Θ is the switching function and it is equal to 1 for the control elements displaying a welded tube in the middle and equal to 0 in the case of edge elements and of elements where tubes are not welded (only in standard collectors, close to the manifold tubes). If Θ is equal to 1, when thermal conduction between elements is not taken into account (first step), the useful heat flux is expressed by the Bliss equation and the energy balance is described in (eq.8):

$$0 = \tau\alpha \cdot G - U_{c\_x,y} \cdot \left(t_p - t_a \right) - \Theta \cdot U_{tp\_x,y} \cdot \left(t_p - t_m \right) \qquad \text{(eq.8).}$$

In (eq.8), the third term on the right represents the useful heat flux which is transferred between the plate and the fluid flowing into the tubes and $U_{tp\_x,y}$ is the heat transfer coefficient between the plate and the fluid and it accounts for the thermal convection of the fluid flow inside the channels. The convective heat transfer coefficient is calculated with equations from Duffie and Beckman (2006). The same energy balance can be written for the second step, when the thermal conduction between different control elements is considered:

$$0 = \tau\alpha \cdot G - U_{c\_x,y} \cdot \left(t_p - t_a \right) + k \cdot \delta \cdot \frac{\partial^2 t_p}{\partial x^2} + k \cdot \delta \cdot \frac{\partial^2 t_p}{\partial y^2} - \Theta \cdot U_{tp\_x,y} \cdot \left(t_p - t_m \right) \qquad \text{(eq.9).}$$

The overall loss coefficient between the plate and the surroundings is the sum of the top, bottom and edge loss coefficient. The top coefficient is related to the free-convection between absorber sheet and glass cover using the model suggested by Hollands et al. (1976) and to the free-convection coefficient with the external surroundings, calculated with two different relationships (McAdams, 1954 and Fujii and Imura, 1972). The McAdams (1954) correlation is related with the wind speed, while the Fujii and Imura (1972) correlation does not account for this parameter. The bottom coefficient considers the conduction heat transfer through the back insulation layer that is depending on the average temperature of insulation, as stated in the standard EN ISO 10456 (2008). For the computation of edge heat losses, the convection and the radiative heat transfer are considered in the zone above the insulation layer, because in the tested collectors there is not lateral insulation. From the fin theory, the collector efficiency factor *F'* and the collector heat removal factor F_R are calculated as reported in Duffie and Beckman (2006) and they are used to obtain the useful heat transfer in the control element. From the computation of these coefficients it is possible to gain a temperature map of the plate with an iterative method.

For each collector, the average ambient air temperature and the average wind speed in the horizontal plane during the tests have been calculated: these values have been used in the simulations. For all the collectors, a global irradiance of G = 1000 W/m^2 and an angle of incidence of 10° are considered. In the simulations of each collector the coefficients necessary for plotting the efficiency of the collector according to (eq.3) were obtained: these coefficients are reported in Table 8.

In Fig. 8-9, the results of the numerical implementation of the model are presented in terms of comparison between the efficiency curves obtained by the experimental measurements in steady-state condition and the efficiency curves obtained by the simulations, using the two different correlations for the external convection. For the experimental curves the experimental uncertainty bands are also given.

The comparisons shows that the Fujii and Imura (1972) correlation is more accurate to predict the behavior of black coated collector, while McAdams (1954) correlation is more accurate to predict the behavior of collector with selective coating. The model prediction is more accurate for collector with selective coating than for collector with black coating. According to the authors, this can be explained considering that at the same working conditions, the glass cover of a selective collector remains at a lower temperature than the one of a black coated collector because the absorber has a lower emittance. Thus, when a selective coating is employed, the wind speed should have a greater influence on the free-convection between glass cover and external surroundings.

Table 8: Collector coefficients obtained from the simulation with the numerical model.

	Standard flat plate collector, copper absorber with black coating, copper tubes		Roll-bond flat plate collector, black coating		Roll-bond flat plate collector, semi-selective coating	
Correlation	McAdams (1954)	Fujii & Imura (1972)	McAdams (1954)	Fujii & Imura (1972)	McAdams (1954)	Fujii & Imura (1972)
η_0	0.6934	0.7086	0.7991	0.8010	0.7422	0.7426
a_1 [[W/(m^{2}K)]	5.9841	5.2067	6.1934	5.2037	4.7240	4.1269
a_2 [W/(m^{2}K)]]	0.0172	0.0194	0.0251	0.0266	0.0168	0.0171

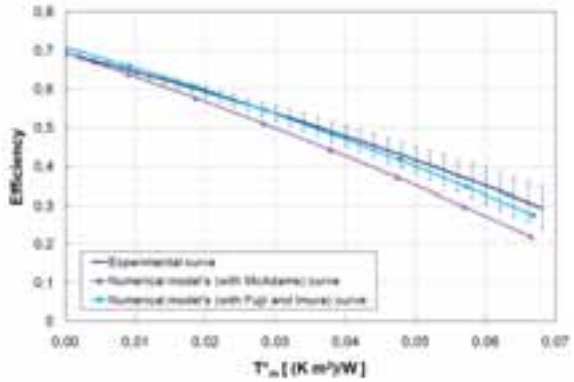

Fig. 8: Comparison between experimental efficiency curves and modeled curves at G = 1000 W/m^2 in steady-state conditions: standard copper collector with black coating.

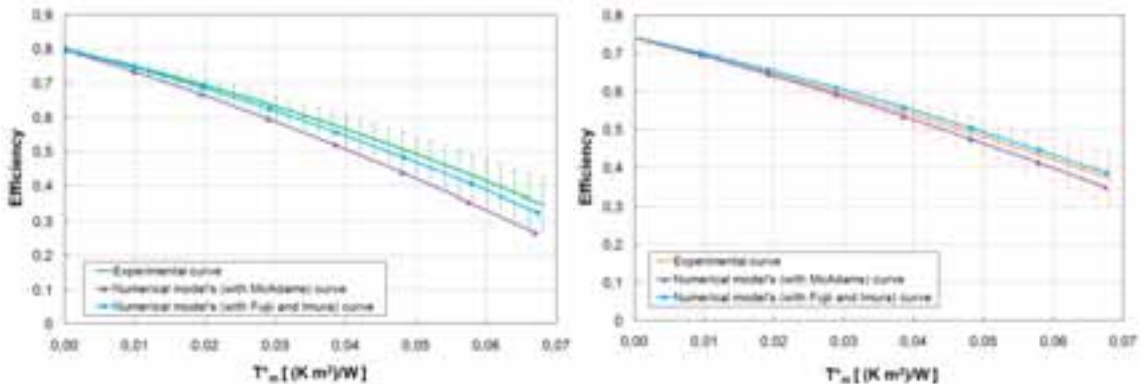

Fig. 9: Comparison between experimental efficiency curves and modeled curves at G = 1000 W/m^2 in steady-state conditions. Left: Roll-bond collector with black coating; Right: Roll-bond collector with semi-selective coating.

5 . Conclusions

A standard glazed flat solar collector with copper black absorber and copper tubes and two new glazed flat solar collectors that use a roll-bond plate as absorber have been characterized following the steady-state and the quasi-dynamic methods reported in the standard EN 12975. The roll-bond collectors are provided with a black coating and a semi-selective coating respectively.

The efficiency curves obtained with steady-state and quasi-dynamic test methods are in agreement within their uncertainties. The experimental results show that the roll-bond collectors are competitive products as compared to standard collectors. In particular, the roll-bond collector with black coating has better performances and a higher efficiency curve than the standard collector with the same paint. Moreover, the black roll-bond collector is more efficient than the reference standard collector with selective coating for reduced temperature $T_m^* < 0.035$ m^2 K/W.

The results obtained from the implementation of the three-dimensional computation model are in good agreement with the experimental efficiency curves. The relationship suggested by Fujii and Imura (1972) for the calculation of the free-convection coefficient between the glass cover and external surroundings is more accurate to predict the behavior of black coated collectors, while McAdams (1954) correlation is more suitable for selective coated collectors.

The present work shows that the use of an aluminum roll-bond plate as absorber can be interesting for the development of new solar collectors with higher performance and lower cost as compared to standard flat plate type.

Nomenclature

A_a	Aperture area of collector	[m^2]
a_1	heat loss coefficient	[W/(m^{2}K)]
a_2	temperature dependence of heat loss coefficient	[W/(m^{2}K)]
b_0	incidence angle modifier coefficient for flat plate collector	-
c_p	specific heat at constant pressure	[J/(kg K)]
c_1	heat loss coefficient	[W/(m^{2}K)]
c_2	temperature dependence of heat loss coefficient	[W/(m^{2}K)]
c_3	wind speed dependence of heat loss coefficient	[(J/m^3 K)]
c_4	long-wave irradiance dependence of heat loss coefficient	[W/(m^{2}K)]
c_5	effective thermal capacitance	[J/(m^{2}K)]
c_6	wind speed dependence in zero loss efficiency	[s/m]
E_L	long-wave irradiance ($\lambda > 3$ μm)	[W/m^2]
F'	collector efficiency factor	-
G	global solar irradiance	[W/m^2]
G_b	direct solar irradiance	[W/m^2]
G_d	diffuse solar irradiance	[W/m^2]
k	thermal conductivity of absorber plate	[W /m K]
$K_{\theta b}$	incidence angle modifier for direct irradiance	-
$K_{\theta d}$	incidence angle modifier for diffuse irradiance	-
$\dot{m}$	mass flow rate	[kg/s]
$\dot{Q}$	useful power extracted from collector	[W]
q_u	useful power extracted from the collector (model)	[W]
T_a	ambient air temperature	[K]
t_a	ambient air temperature	[°C]
t_{in}	inlet fluid temperature	[°C]
t_m	mean fluid temperature	[°C]
T_m^*	reduced temperature difference	[m^2 K/W]
t_{out}	outlet fluid temperature	[°C]
t_p	absorber plate temperature	[°C]
u	surrounding air speed	[m/s]
U_c	overall heat loss coefficient	[W/(m^{2}K)]
U_{tp}	heat transfer coefficient between plate and fluid	[W/(m^{2}K)]
w	spacing between tubes	[m]

Subscripts

x	position transversal to tube axis
y	position along tube axis

Greek symbols

δ	thickness of absorber plate	[m]
η	efficiency	
η_0	zero loss collector efficiency	-
σ	Stefan-Boltzmann constant	[W/m^{2}K^4]
$(\tau\alpha)$	transmittance-absorbance product	-
$(\tau\alpha)_{en}$	transmittance-absorbance product at normal incidence	-
θ	angle of incidence	[°]
Θ	switching function (0 or 1)	-
τ	time	[s]

Acknowledgments

The authors would like to acknowledge the financial support of Riello SpA, Legnago (VR), Italy. The financial support of the Regione Veneto through the project FSE 2105/1/6/1102/2010 is also acknowledged.

References

Drummond A.J., 1956. On the measurements of sky radiation. Archiv für Meterorologie Geophysik und Bioklimatologie 7, 413-436

Duffie, A., Beckman, W.A., 2006. Solar engineering of thermal processes, 3rd ed., Wiley&Sons, New Jersey

EN 12975, 2006. European Standards. Thermal solar system and components- Solar collector- Part 2: Test methods.

EN ISO 10456, 2007. International Standard. Building materials and product- Hygrothermal properties- Tabulated design values and procedure for determining declared and design thermal values.

Fujii T., Imura H., 1972. Natural-convection heat transfer from a plate with arbitrary inclination. International Journal of Heat and Mass Transfer, 15, 755-767.

ISO, 1995. Guide to the Expression of Uncertainty in Measurement.

Hollands, K.G.T., Unny, T.E., Raithby, G.D.,Konicek, L.,1976. Free convection heat transfer across inclined air layers. Trans. ASME, J. Heat Transfer, 98, 189.

Kratzemberg, M.G., Beyer H.G., Colle S., 2006. Uncertainty calculation applied to different regression method in the quasi-dynamic collector test. Solar Energy, 80, 1453-1460.

Liu B.Y.H., Jordan, R.C., 1963. The long-term average performance of flat plate solar energy collectors. Solar Energy, 7.

McAdams, W.H.,1954, Heat transmission, 3rd ed.,McGraw-Hill, New York.

Test report SPF, “Solar Collector Factsheet Riello CP20TS”, 2008. Available at *http://www.spf.ch/*

Zambolin, E., Del Col, D.,2010 a. Development and experimental validation of a numerical model for flat plate solar collectors. In: Heat SET 2010.

Zambolin, E., Del Col, D., 2010 b. Experimental analysis of thermal performance of flat plate and evacuated tube collectors in stationary standard and daily conditions. Solar Energy,84, 1382-1396.